Addressing Low-Contrast Challenges: A Context-Aware Segmentation Algorithm For Robust 3D Lumbar Spine Reconstruction From Standard CT

Xuemei Wang[12]

[1] *School of Information Engineering, Shandong Huayu University of Technology, DeZhou, China, 253034*
[2] *Department of Information Technology, Pavel Sukhoi State Technical University of Gomel, Gomel, Belarus,246029*
[1*] *Corresponding author. E-mail: Xuemeiwang37@outlook.com*

Received July 22, 2026; accepted Aug. 24, 2026

Medical imaging through Computed Tomography (CT) performs critical functions because it provides essential support for both diagnosing and developing treatment plans for spinal disorders. The process of preoperative planning and surgical procedures depends on accurate lumbar spine segmentation together with 3D reconstruction of CT images. The process of lumbar spine segmentation faces major difficulties which arise from three factors: low-contrast areas, imaging artifacts, and different anatomical structures. The current methods are unable to solve these operational obstacles because they produce results with both reduced precision and diminished productivity. The research presents a new solution with its Context-Aware 3D Attention U-Net model which combines the Marine Predators Algorithm (MPA) for feature selection optimization. unnecessary elements while boosting learning efficiency. A hybrid loss function which combines include intensity normalization and resampling and Region of Interest (ROI) cropping to produce high-quality data input. The post-processing stage enhances segmentation output through processes which produce a seamless 3D reconstruction. The proposed model demonstrates superior performance compared to baseline methods while achieving a Dice score of 0.951 and an IoU of 0.907 and a precision of 0.963 and a recall of 0.944. The boundary error (HD95) measurement shows significant improvement because it decreased to 2.18 mm, which indicates better segmentation results and boundary detection performance. The method provides an accurate lumbar spine segmentation solution that people can use across various clinical settings which involve low-contrast CT scans.

Keywords: Lumbar spine segmentation, 3D reconstruction, Context-Aware 3D Attention U-Net, Marine Predators Algorithm, feature selection.

© The Author('s). This is an open-access article distributed under the terms of the Creative Commons Attribution License (CC BY 4.0), which permits unrestricted use, distribution, and reproduction in any medium, provided the original author and source are cited.

http://dx.doi.org/10.6180/jase.202612_35.070

1. Introduction

Medical imaging serves essential functions in three key areas which include diagnosing spinal disorders and creating treatment plans as well as assisting in surgical operations [1]. CT emerges as the most effective imaging method since it provides exceptional detail for examining bony structures throughout the lumbar spine (L1–L5) region [2]. The clinical field needs accurate lumbar vertebrae segmentation together with 3D reconstruction because these processes enable various medical functions which include preoperative planning and spinal alignment assessment and implant positioning and fracture detection. Computer-aided diagnosis systems have enhanced modern healthcare systems by increasing their ability to support medical decision-making processes [3]. The process of manually segmenting verte-

brae from volumetric CT data requires extensive labour and takes a long time to complete while results show different levels of accuracy between observers [4].

The examination of lumbar spine analysis remains difficult because of multiple factors which continue to exist despite current technological developments. The different dimensions and shapes of vertebrae which each patient possesses create major difficulties because of their complex anatomical structure [5]. The system experiences problems with segmentation because of two different factors which include low tissue contrast and imaging artifacts and noise and partial volume effects [6]. The presence of osteoporosis and disc degeneration and spinal stenosis and fractures causes further vertebral structure distortion which makes boundary delineation more difficult [7]. The analysis of 3D CT volumes which contain high-dimensional data needs extensive computational power which results in greater memory needs and longer training durations.

The development of multiple Deep Learning (DL) based segmentation techniques which include 2D U-Net 3D U-Net and Attention U-Net architectures has been initiated to solve these problems [8]. Most current methods use raw voxel intensities for analysis without using optimized feature selection systems which results in unnecessary feature extraction.

Tao et al. [9] created, functions as a context-aware system that enables 2D and 3D vertebra tracking through its ability to monitor spatial connections between multiple slices. The method shows that contextual learning needs to be developed for better spine analysis which depends on accurate identification of vertebral structures. The method shows that complete 3D spinal structure reconstruction remains achievable through the use of minimal projection data yet the technique requires X-ray imaging which functions differently than volumetric reconstruction methods that use CT imaging.

Hayat and Z. Yuqian [10] created MSAE-U-Net, which functions as a multiscale attention-based U-Net system to segment abdominal cancer cases. Their approach shows that attention mechanisms combined with multiscale feature extraction methods can enhance segmentation accuracy, which proves essential for processing medical images that have low contrast. Abel et al. [11] studied DL methods for 3D lumbar spine MRI reconstruction which they used in surgical planning. The study proves that reconstructed MRI volumes reach CT measurement precision which shows the clinical advantages of 3D reconstruction techniques. Haida et al. [12] developed a combined three-dimensional robotic system which they used to demonstrate how 3D imaging technology benefits actual surgical procedures. Their research demonstrates how medical facilities are implementing advanced imaging methods for use during actual patient treatment. Altorfer et al. [13] investigated robotic pedicle screw placement through 3D MRI registration methods to minimize radiation exposure during spine surgery. The research demonstrates that accurate 3D spine models have become essential for directing surgical procedures. The existing reconstruction methods that use sparse X-ray information cannot make use of all the volumetric CT data according to research [14]. The attention-based segmentation models feature representation capabilities but they do not provide the optimal solution for processing low-contrast CT images. Current 3D reconstruction research depends mainly on MRI data which has different properties compared to CT imaging modalities according to research.

2. Materials and methods

The proposed framework for lumbar spine segmentation and 3D reconstruction begins with data collection from the CTSpine1K dataset, followed by pre-processing steps like HU windowing, resampling to uniform voxel spacing, and ROI cropping. The team extracts intensity, texture, and spatial features, segments using Context-Aware 3D Attention U-Net, refines, stacks slices, applies Marching Cubes, and assesses performance in Figure 1.

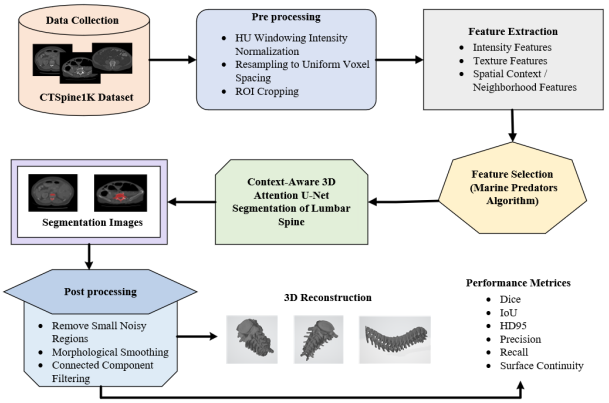


Fig. 1. The Overall Proposed Work

2.1. Feature Extraction

Feature extraction derives informative voxel-level characteristics from CT images to improve segmentation accuracy using intensity, texture, and spatial context features for precise lumbar vertebrae detection. Low-contrast CT characteristics make direct voxel discrimination difficult because vertebral and surrounding tissue intensities can overlap. The combined HU intensity, GLCM and Gabor

texture, and spatial context features provide complementary information for distinguishing vertebral structures and maintaining anatomical continuity. These selected features support contextual learning in the Context-Aware 3D Attention U-Net for accurate lumbar vertebrae segmentation.

2.1.1. Intensity Features (HU)

Voxel-level intensity features are derived directly from HU values in CT images, representing tissue radiodensity and differentiating bone from soft tissues through higher intensity ranges, preserving HU information for effective spine segmentation.

2.1.2. Texture Features (GLCM and Gabor)

Texture features characterize intensity variations across adjacent image regions, providing structural information through GLCM contrast, correlation, homogeneity, while Gabor filters extract texture across various scales and orientations. Gabor filters used 4 orientations (0°, 45°, 90°, 135°) and 3 scales with spatial frequencies of 0.05, 0.10, and 0.20 cycles/voxel, producing 12 filter responses. Kernel size was 15 × 15, Gaussian bandwidth was 4, aspect ratio was 0.5, and feature aggregation used mean magnitude. The GLCM-derived contrast, correlation, and homogeneity features characterize local intensity relationships within vertebral regions, helping distinguish consistent vertebral texture patterns from surrounding tissues in challenging anatomical regions. These texture characteristics support the identification of vertebral structures were low contrast complex anatomical boundaries.

2.1.3. Spatial Context / Neighbourhood Features

Spatial context features use information from nearby voxels to trace anatomical continuity and identify structural connections, preserving structures and reducing errors in ambiguous anatomical regions. The selected HU intensity, GLCM texture, Gabor filter responses, and neighbourhood information collectively represent lumbar vertebral characteristics through complementary intensity, texture, edge, and spatial information. HU, GLCM, and Gabor features capture radiodensity, texture, and edge information, while neighbourhood information preserves spatial continuity. This combined representation enhances contextual feature learning and vertebral boundary identification during low-contrast CT segmentation.

2.2. Feature Selection Using MPA

MPA selects essential features from high-dimensional lumbar CT data, reducing redundant information and computational costs while improving segmentation accuracy.

2.2.1. Overview of MPA

MPA is a metaheuristic optimization algorithm inspired by the foraging behaviour of marine predators. The process starts with the creation of solution process uses position update formula to iteratively improve each solution until it reaches the elite status in Eq. (1)

$$X_i^{t+1} = X_i^t + R \cdot \left(\text{Elite}^t - X_i^t\right) \tag{1}$$

Here, X_i^t is current solution, Elite^t is best solution at iteration t, R is random vector controlling movement. MPA selects informative combinations of HU intensity, GLCM texture, Gabor filter responses, spatial context features for lumbar spine segmentation. The candidate subsets optimized through exploration exploitation, while fitness function considers segmentation error feature count reduce redundant features. The selected feature subset then provided Context-Aware 3D Attention U-Net lumbar vertebrae segmentation.

2.2.2. Lévy Flight and Brownian Motion for Global Search

The algorithm uses Brownian motion for local exploration and Lévy flight for global exploration. The Lévy flight method permits extended space exploration which enables the algorithm to investigate different feature combinations in Eqn. (2)

$$\text{Step} = \alpha \cdot \frac{u}{|v|^{1/\beta}} \tag{2}$$

where u and v are random variables, β defines Lévy distribution, α is a scaling factor.

2.2.3. Fitness Evaluation and Optimization

The fitness function evaluates quality of each candidate feature subset through its assessment of segmentation accuracy together with its measurement of feature count in Eqn. (3)

$$\text{Fitness} = \lambda \cdot \text{Error} + (1 - \lambda) \cdot \frac{|F_{\text{selected}}|}{|F_{\text{total}}|} \tag{3}$$

where Error represents segmentation error, $|F_{\text{selected}}|$ is number of selected features, $|F_{\text{total}}|$ total number of features, and λ balances accuracy and feature reduction.

The MPA used 30 solutions over 50 iterations, with exploration, transition, and exploitation phases of 0–16, 17–33, and 34–50 iterations. Brownian and Lévy coefficients were 1 and 0.01, with $\lambda = 0.1$, a binary threshold of 0.5, and bounds [0,1]. Convergence used a tolerance of 1×10^{-4} and 10-iteration patience, stopping at 50 iterations or convergence.

2.3. Context-Aware 3D Attention U-Net Segmentation of Lumbar Spine

Medical image segmentation uses U-Net-based architectures, with 3D Attention U-Net expanding 64 to 512 channels, final convolution for CT segmentation in Figure 2. The integration of MPA with the Context-Aware 3D Attention U-Net is motivated by their complementary functions, where MPA selects informative intensity, texture, spatial features, context attention mechanisms capture multi-scale anatomical relationships and emphasize relevant vertebral regions. This combination reduces redundant feature information before segmentation, enabling focus on discriminative lumbar structures for low-contrast CT segmentation. The selected features are passed to Context-Aware 3D Attention U-Net for lumbar vertebrae segmentation. The refined segmentation undergoes post-processing to improve segmented mask before reconstruction. The processed segmented slices are then reconstructed using Marching Cubes algorithm to generate final 3D lumbar spine model.

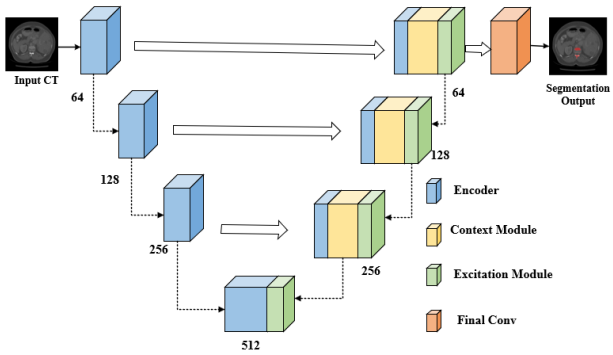


Fig. 2. *Architecture of 3D Attention U-Net for CT Image Segmentation*

The context module processes the input to extract multi-scale relationships together with worldwide contextual information which it shows in Eqn. (4)

$$F_c = f_{\text{context}}(F_e) = \sum_{s=1}^{S} W_s * F_e^{(s)} \tag{4}$$

The number of scales is S while $F_e^{(s)}$ serves as feature map which exists at scale s. The network needs to concentrate its processing power on important spinal areas through the use of an attention gate which generates attention coefficients Eqn. (5)

$$\alpha = \sigma\left(W_{\text{att}}^{T}(F_c + F_d) + b_{\text{att}}\right) \tag{5}$$

The network is trained using a combination of Dice, Focal, and Boundary loss functions. The combined loss is defined as in Eqn. (6)

$$\mathcal{L} = \lambda_1 \mathcal{L}_{\text{Dice}} + \lambda_2 \mathcal{L}_{\text{Focal}} + \lambda_3 \mathcal{L}_{\text{Boundary}} \tag{6}$$

The hybrid loss function assigns weights of 0.5 to Dice Loss, 0.3 to Focal Loss, and 0.2 to Boundary Loss, with a total weight of 1. The weighted combination addresses class imbalance and improves edge detection, contributing to accurate lumbar spine segmentation.

Algorithm 1. Context-Aware 3D Attention U-Net for Lumbar Spine Segmentation

Require: 3D CT volume X
Ensure: Segmented mask Y_{pred}
Initialize model parameters
for epoch $= 1$ **to** N **do**
  for all input X **do**
    Encoder
    $F_e = \text{Conv3D}(X)$
    Context module
    $F_c = \text{Multiscale}(F_e)$
    Attention
    $F_e = \text{Sigmoid}(F_c)$
    $F_{\text{att}} = \alpha \cdot F_c$
    Decoder
    $F_d = \text{UpSample}(F_{\text{att}})$
    # Output
    $Y_{\text{pred}} = \text{Sigmoid}(F_d)$
    Loss
    Loss $=$ Dice $+$ Focal $+$ Boundary
    Update
    Update weights using Adam

2.4. Post processing

Post-processing refines the segmented mask by removing noise, smoothing irregular boundaries, and filtering disconnected components. Morphological smoothing uses opening and closing operations to remove minor disturbances, fill small gaps, improve boundary smoothness. Connected-component filtering removes non-lumbar small isolated regions, preserving L1–L5 vertebral mask continuity before three-dimensional reconstruction.

2.4.1. Connected Component Filtering

The connected-component analysis examines each segmented mask to identify the regions to lumbar vertebrae L1–L5. The components of the system $\{C_1, C_2, \ldots, C_n\}$ in Eqn. (7)

$$M' = \bigcup_{i=1}^{k} C_i^{\text{sorted}} \tag{7}$$

The prediction and binary mask thresholds are set to 0.5, with a 26-connected neighbourhood used for connected component filtering. Components smaller than 500 voxels are removed, upto 5 components are retained based volume anatomical centroid, $3 \times 3 \times 3$ morphological kernel one opening one closing iteration with 3D hole filling preserve vertebral structures.

2.5. Data Collection

The CTSpine1K dataset [15] is used as the main dataset because it contains more than 1000 three-dimensional CT volumes with vertebra-level annotations.

Figure 3 presents representative lumbar spine CT images with varying contrast and clarity as input data, supporting subsequent segmentation and 3D reconstruction processes.

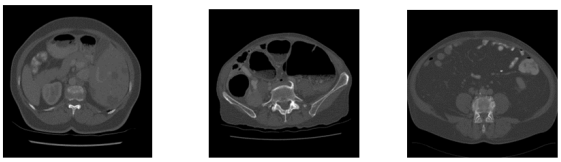


Fig. 3. presents representative lumbar spine CT images with varying contrast and clarity as input data, supporting subsequent segmentation and 3D reconstruction processes.

2.6. Data Pre-processing

2.6.1. HU Windowing (Bone Window)

Bone-specific HU windowing enhances vertebral contrast by highlighting bony structures and segmentation. The transformation is defined as in Eqn. (8)

$$I_{\text{window}}(x) = \begin{cases} L, & I(x) < L \\ I(x), & L \leq I(x) \leq U \\ U, & I(x) > U \end{cases} \tag{8}$$

The process establishes two limits which are L for the lower bound and U for the upper bound of the bone window. Bone-window HU preprocessing used a window level of 300 HU and width of 1500 HU, corresponding to a range of -450 to 1050 HU, followed by min–max normalization to $[0, 1]$ and $1 \times 1 \times 1$ mm resampling.

2.6.2. Resampling to Uniform Voxel Spacing

The 3D convolutional operations experience negative effects from these inconsistencies. The resampling operation is given by Eqn. (9)

$$x' = x \cdot \frac{s_{\text{orig}}}{s_{\text{target}}}, \quad I_{\text{resampled}}(x') = I(x) \tag{9}$$

where s_{orig} and s_{target} indicates the original and intended voxel spacing.

2.6.3. ROI Cropping (Lumbar Region Extraction)

ROI cropping extracts the lumbar spine (L1–L5) region, reducing computational cost and enabling model to focus on clinically relevant structures for segmentation shows in Eqn. (10)

$$I_{\text{ROI}} = I(x), x \in \Omega_{\text{lumbar}} \tag{10}$$

The spatial area which contains lumbar vertebrae is defined by the term Ω_{lumbar}.

The ROI targets the L1–L5 lumbar vertebrae using a 3D bounding-box strategy based on vertebral annotations, with a 10-voxel margin retained around the selected region. After resampling to $1 \times 1 \times 1$ mm spacing, the ROI dimensions are fixed at $160 \times 160 \times 128$ voxels, corresponding to a physical size of $160 \times 160 \times 128$ mm^3.

2.7. Hardware Software Requirements

The proposed framework was implemented on an Intel® Core™ i9-14900K system with 32 GB RAM and Windows 11 Home using Python-based DL and medical imaging libraries.

2.8. Hyperparameter Configuration of the Proposed 3D Attention U-Net Model

The Adam optimizer with a learning rate of 0.0001 and weight decay of 1.00×10^{-5} supports stable optimization and efficient convergence. ReduceLROnPlateau with 10-epoch patience regulates learning when validation improvement plateaus, while batch size 2 and a maximum of 100 epochs provide controlled training of the 3D CT volumes. Training and validation losses and Dice score were monitored, with early stopping after 20 epochs without sufficient validation improvement to maintain convergence and training stability.

3. Results and discussion

The proposed Context-Aware 3D Attention U-Net with MPA significantly outperforms 2D U-Net segmentation 3D reconstruction metrics, statistically superior performance.

The computational complexity is characterized by 18.7 M trainable parameters and 112.6 G FLOPs, while execution time is 3.8 min per epoch, 6.3 h for total training, 0.84 s per 3D volume, and 18.5 ms per slice, with GPU memory usage of 7.8 GB.

Table 1. Ablation Analysis of Individual Components of the Proposed Model

Model Configuration	Dice	IoU	Precision	Recall	HD95 (mm)
Without Context Module	0.936	0.881	0.950	0.928	2.91
Without Attention Mechanism	0.941	0.889	0.955	0.934	2.68
Without MPA	0.925	0.872	0.938	0.918	3.96
Without Hybrid Loss	0.929	0.875	0.944	0.922	3.51
Full Proposed Model	**0.951**	**0.907**	**0.963**	**0.944**	**2.18**

Table 2. Segmentation Performance Across Different Segmentation Scenarios

Segmentation scenario	Dice	IoU	Precision	Recall	HD95 (mm)
Standard contrast	0.951	0.907	0.963	0.944	2.18
Mild low contrast	0.945	0.896	0.958	0.938	2.39
Severe low contrast	0.927	0.865	0.944	0.916	3.01
Noise-degraded	0.923	0.856	0.941	0.913	3.14
Boundary ambiguity	0.932	0.872	0.949	0.920	2.94
Anatomical variation	0.931	0.871	0.948	0.919	2.96

3.1. Feature Importance

The MPA Selected Features show the key features influencing the segmentation process.

Figure 4 shows that the MPA identifies Gradient as the most influential feature, followed by Neighbourhood, Gabor, GLCM Texture, and HU Intensity, improving segmentation accuracy.

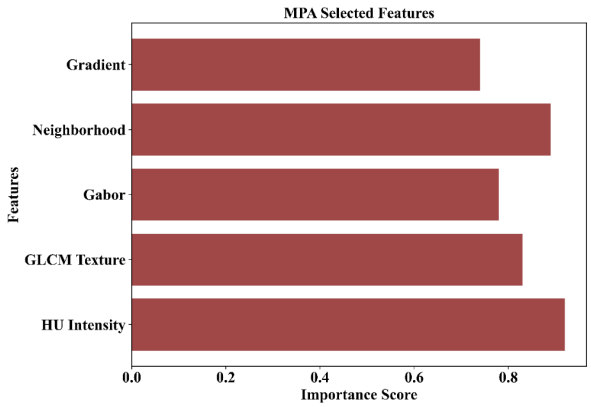


Fig. 4. shows that the MPA identifies Gradient as the most influential feature, followed by Neighbourhood, Gabor, GLCM Texture, and HU Intensity, improving segmentation accuracy.

Table 1 shows the Full Proposed Model achieves Dice 0.951, IoU 0.907, Precision 0.963, Recall 0.944, HD95 2.18 mm, outperforming Individual Components ablated configurations.

3.2. Segmentation of CT Slice 348

The Segmentation of CT Slice 348 shows the progression from the original CT image to the ground truth mask, predicted mask and the overlay of the predicted mask on the original image

Figure 5 displays the unprocessed CT slice, ground truth mask, predicted mask, and predicted mask overlaid on the original CT slice, showing segmentation accuracy.

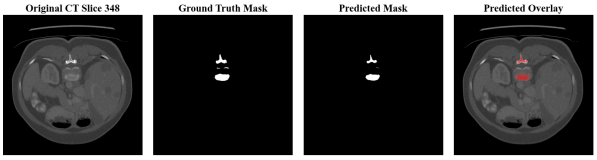


Fig. 5. displays the unprocessed CT slice, ground truth mask, predicted mask, and predicted mask overlaid on the original CT slice, showing segmentation accuracy.

Table 2 shows segmentation performance across scenarios, with Dice 0.951–0.923, IoU 0.907–0.856, Precision 0.963–0.941, Recall 0.944–0.913, and HD95 2.18–3.14 mm.

3.3. Robustness to Low Contrast

The Segmentation Robustness to Low-Contrast shows how well the model maintains its segmentation results when facing different contrast situations.

Table 3 demonstrates robustness across CT conditions, with overall Dice 0.941, IoU 0.884, and HD95 2.91 mm; standard CT achieved Dice 0.951, while artifacts yielded

Table 3. Robustness Evaluation Under Different CT Image Quality, Scanning Conditions and Patient Anatomy

CT condition / subgroup	N	Dice	IoU	Precision	Recall	HD95 (mm)
Standard-quality CT	80	0.951	0.907	0.963	0.944	2.18
Low-contrast CT	30	0.927	0.865	0.944	0.916	3.01
High-noise CT	25	0.923	0.856	0.941	0.913	3.14
Artifact-affected CT	20	0.918	0.849	0.936	0.907	3.28
Anatomically challenging cases	25	0.931	0.871	0.948	0.919	2.96
Overall	180	0.941	0.884	—	—	2.91

0.918.

3.4. Model Performance and Comparison

The 3D Segmentation Comparison of Different Models shows all other segmentation methods.

Table 4 demonstrates that the proposed Context-Aware 3D Attention U-Net significantly outperforms baseline models across all segmentation and 3D reconstruction metrics ($p < 0.05$).

3.5. 3D Reconstruction Quality

The 3D Reconstruction of Lumbar Spine Segmentation shows how segmentation evolved from its initial fragmented state to reach complete 3D reconstruction accuracy. The Marching Cubes algorithm converts the stacked segmented volume into a three-dimensional surface representation. It establishes connectivity between neighboring voxels to generate a continuous surface across the segmented lumbar vertebrae. This process preserves the anatomical surface continuity required for accurate 3D lumbar spine reconstruction.

Table 5 presents the reconstructed lumbar spine validation, achieving surface continuity of 0.952, anatomical continuity 96.1%, reconstruction success 98.4%, expert agreement $\kappa = 0.89$.

The improved performance in low-contrast CT images is attributed to the context-aware and attention mechanisms, which capture spatial relationships across the 3D volume and emphasize relevant vertebral regions.

Table 6 compares lumbar spine CT segmentation methods, with proposed method achieving highest Dice 0.951, IoU 0.907, precision 0.963, recall 0.944, and lowest HD95 2.18 mm.

Table 7 validates external generalization, with the External Test achieving Dice 0.934, IoU 0.879, Precision 0.951, Recall 0.928, and HD95 2.74 mm, versus internal results.

Table 8 reports Dice 0.951, external Dice 0.934, worst-case Dice 0.918, HD95 2.18–3.28 mm, 18.7 M parameters, 7.8 GB memory, 0.84 s inference, and 96.10% continuity.

3.6. Discussion

The proposed Context-Aware 3D Attention U-Net outperformed conventional 2D U-Net and 3D U-Net models for lumbar spine segmentation 3D reconstruction, achieving superior Dice score, IoU, Precision, Recall, and HD95 metrics. MPA feature selection and hybrid loss improved segmentation accuracy, reduced boundary errors, enhanced 3D structural continuity, anatomical accuracy, and robustness.

4. Conclusion and future work

This research proposes a Context-Aware 3D Attention U-Net integrated with the Marine Predators Algorithm (MPA) for accurate lumbar spinal segmentation and three-dimensional reconstruction from low-contrast CT scans. By combining optimized feature selection, attention mechanisms, and advanced pre- and post-processing techniques, the framework achieves robust performance under challenging imaging conditions such as low contrast, noise, and structural variations. The Context-Aware 3D Attention U-Net enhances the segmentation process by learning multi-scale spatial relationships and emphasizing clinically relevant vertebral regions through attention mechanisms. In addition, the hybrid loss function consisting of Dice, Focal, and Boundary losses improves the handling of class imbalance and boundary delineation. The subsequent morphological processing and connected-component filtering refine the segmentation masks by removing isolated regions, reducing noise, and preserving the continuity of L1–L5 vertebral structures. Experimental results show significant improvements over the baseline model, increasing the Dice score from 0.925 to 0.951, IoU from 0.872 to 0.907, and improving Precision and Recall while reducing the HD95 boundary error from 3.96 mm to 2.18 mm. The model also maintains strong performance on low-contrast images, and future work will focus on integrating MRI data and developing real-time clinical tools for surgical planning and evaluation.

Table 4. Statistical Comparison Between Baseline and Proposed Model Metrics

Metric	Baseline Mean	Proposed Mean	t-value	p-value	Significant ($p < 0.05$)
Dice Score	0.93	0.951	5.21	0.0003	Yes
IoU	0.87	0.907	4.87	0.0006	Yes
Precision	0.947	0.963	4.12	0.0011	Yes
Recall	0.915	0.944	4.45	0.0009	Yes
HD95 (mm)	3.28	2.18	5.78	0.0002	Yes
Surface Continuity	0.9	0.95	4.63	0.0007	Yes
Visual Smoothness	0.89	0.94	4.28	0.0009	Yes
Structural Integrity	0.88	0.93	4.51	0.0008	Yes

Table 5. Anatomical and Clinical Validation of Reconstructed Lumbar Spine

Validation measure	Obtained Value
Surface continuity	0.952
Surface smoothness	0.941
Structural integrity	0.934
Anatomical continuity rate	96.10%
Mean vertebral centroid error	1.72 mm
Mean vertebral height error	1.84 mm
Mean vertebral width error	2.11 mm
Intervertebral distance error	1.96 mm
Mean surface-to-surface distance	1.87 mm
Vertebral identification accuracy (%)	97.3
Anatomical continuity (%)	96.1
Reconstruction success rate (%)	98.4
Clinical visualization acceptability (1–5)	4.72 ± 0.21
Vertebral morphology preservation (1–5)	4.65 ± 0.24
Spinal alignment preservation (1–5)	4.61 ± 0.27
Surface reconstruction quality (1–5)	4.68 ± 0.23
Overall clinical usefulness (1–5)	4.69 ± 0.22
Expert agreement (Cohen's κ)	0.89

Table 6. Comparison of Lumbar Spine CT Segmentation Methods

Method	Architecture	Dice	IoU	Precision	Recall	HD95 (mm)
U-Net [16]	2D CNN	0.842	0.731	0.856	0.828	6.25
nnU-Net [17]	Self-configuring 3D CNN	0.903	0.795	0.912	0.897	4.35
3D Multi-object CNN	3D CNN	0.921	0.854	0.934	0.914	3.02
VerFormer	Transformer-based	0.928	0.866	0.941	0.919	2.87
Proposed Method	**Context + Attention + MPA**	**0.951**	**0.907**	**0.963**	**0.944**	**2.18**

Table 7. External Dataset Validation

Dataset	Evaluation Set	Dice	IoU	Precision	Recall	HD95 (mm)
CTSpine1K	Internal Test	0.951	0.907	0.963	0.944	2.18
External Dataset	External Test	0.934	0.879	0.951	0.928	2.74

Table 8. Experimental Validation of the Proposed Context-Aware 3D Attention U-Net

Evaluation aspect	Obtained Value
Internal test Dice	0.951
External validation Dice	0.934
Worst-case robustness Dice	0.918
Internal HD95	2.18 mm
External HD95	2.74 mm
Worst-case HD95	3.28 mm
Trainable parameters	18.7 M
GPU memory	7.8 GB
Inference time/volume	0.84 s
Anatomical continuity	96.10%

4.1. Limitations

- The model may struggle with CT images that contain high levels of noise and artifacts because these elements disrupt its ability to accurately segment the images.
- The model faces limitations in practical use because its computational needs exceed what resource-limited environments can provide.

Acknowledgement

The author would like to acknowledge the support provided by the School of Information Engineering, Shandong Huayu University of Technology, China, and the Department of Information Technology, Pavel Sukhoi State Technical University of Gomel, Belarus, for academic and research support during this study.

Declaration

Data availability

alexanderdann/CTSpine1K at main

Conflicts of interest

The author declares that there are no conflicts of interest regarding the publication of this manuscript.

Funding statement

Funding: Dezhou Big Data and Intelligent Perception Technology Engineering Research Center Platform number: PT2025KJT002

Author contribution

Xuemei Wang conceived the study, designed the methodology, performed data analysis, developed the segmentation framework, interpreted the results, and prepared the manuscript.

Ethical approval

This study used publicly available imaging datasets and did not involve direct experimentation on human participants or animals. Therefore, ethical approval was not required.

Consent to participate

Not applicable.

Consent for Publication

Not applicable.

Competing Interests

The author declares that there are no competing interests.

Code Availability

The code developed for the proposed Context-Aware 3D Attention U-Net framework and optimization procedures is available from the corresponding author upon reasonable request.

References

[1] H. Xie, Z. Chen, J. Zhang, and T. Tan, (2025) *"Multi-scale context U-net for breast cancer postoperative radiotherapy in patients with brachial plexus"* **BMC Medical Imaging *26***(1): 8. DOI: 10.1186/s12880-025-02078-1.

[2] W. Wang et al., (2024) *"Transforaminal posterior lumbar interbody fusion microscopic safe operating area: a three-dimensional model study based on computed tomography imaging"* **Journal of Orthopaedic Surgery and Research *19***(1): 342. DOI: 10.1186/s13018-024-04830-9.

[3] A. Gubian et al., (2022) *"CT-Navigated Spinal Instrumentations–Three-Dimensional Evaluation of Screw Placement Accuracy in Relation to a Screw Trajectory Plan"* **Medicina *58***(9): 1200. DOI: 10.3390/medicina58091200.

[4] A. Chan, E. Parent, J. Mahood, and E. Lou, (2022) *"3D ultrasound navigation system for screw insertion in posterior spine surgery: a phantom study"* **International Journal of Computer Assisted Radiology and Surgery *17***(2): 271–281. DOI: 10.1007/s11548-021-02516-9.

[5] Y.-W. Jiang, X.-J. Xu, R. Wang, and C.-M. Chen, (2022) *"Radiomics analysis based on lumbar spine CT to detect osteoporosis"* **European Radiology *32***(11): 8019–8026. DOI: 10.1007/s00330-022-08805-4.

[6] A. Poilliot, M. H.-P. Gay-Dujak, and M. Müller-Gerbl, (2023) *"The quantification of 3D-trabecular architecture of the fourth cervical vertebra using CT osteoabsorptiometry and micro-CT"* **Journal of Orthopaedic Surgery and Research** ***18***(1): 297. DOI: 10.1186/s13018-023-03760-2.

[7] H. Frisk et al., (2024) *"Automatic image registration on intraoperative CBCT compared to Surface Matching registration on preoperative CT for spinal navigation: accuracy and workflow"* **International Journal of Computer Assisted Radiology and Surgery** ***19***(4): 665–675. DOI: 10.1007/s11548-024-03076-4.

[8] B. Saravi et al., (2023) *"Synthetic 3D Spinal Vertebrae Reconstruction from Biplanar X-rays Utilizing Generative Adversarial Networks"* **Journal of Personalized Medicine** ***13***(12): 1642. DOI: 10.3390/jpm13121642.

[9] R. Tao et al., (2026) *"X2P-Net: Context-Aware 2D/3D Vertebra Localization"* **Bioengineering** ***13***(2): 178. DOI: 10.3390/bioengineering13020178.

[10] F. Hayat and Z. Yuqian, (2026) *"MSAE-Unet: a multiscale attention-enhanced U-Net network for abdominal cancer segmentation using deep learning"* **Network Modeling Analysis in Health Informatics and Bioinformatics** ***15***(1): 48. DOI: 10.1007/s13721-025-00684-1.

[11] F. Abel et al., (2024) *"Deep-learning reconstructed lumbar spine 3D MRI for surgical planning: pedicle screw placement and geometric measurements compared to CT"* **European Spine Journal** ***33***(11): 4144–4154. DOI: 10.1007/s00586-023-08123-3.

[12] D. M. Haida et al., (2024) *"Hybrid-3D robotic suite in spine and trauma surgery - experiences in 210 patients"* **Journal of Orthopaedic Surgery and Research** ***19***(1): 565. DOI: 10.1186/s13018-024-05044-9.

[13] F. C. S. Altorfer et al., (2025) *"Robotic pedicle screw placement with 3D MRI registration: moving towards radiation free robotic spine surgery"* **The Spine Journal** ***25***(5): 1035–1041. DOI: 10.1016/j.spinee.2024.10.020.

[14] A. Bayat et al., (2022) *"Anatomy-Aware Inference of the 3D Standing Spine Posture from 2D Radiographs"* **Tomography** ***8***(1): 479–496. DOI: 10.3390/tomography8010039.

[15] *CTSpine1K*. 2026. URL: https://huggingface.co/datasets/alexanderdann/CTSpine1K/tree/main/raw_data/volumes (visited on 03/03/2026).

[16] J. Chen et al., (2024) *"TransUNet: Rethinking the U-Net architecture design for medical image segmentation through the lens of transformers"* **Medical Image Analysis** ***97***: 103280. DOI: 10.1016/j.media.2024.103280.

[17] F. Isensee, P. F. Jaeger, S. A. A. Kohl, J. Petersen, and K. H. Maier-Hein, (2021) *"nnU-Net: a self-configuring method for deep learning-based biomedical image segmentation"* **Nature Methods** ***18***(2): 203–211. DOI: 10.1038/s41592-020-01008-z.